

Constrained Hamiltonian systems and Physics Informed Neural Networks: Hamilton-Dirac Neural Nets

Dimitrios A. Kaltsas ^{*1,2}

¹Department of Physics, University of Ioannina, Ioannina, Greece

²Department of Physics, International Hellenic University, Kavala, Greece

Abstract

The effectiveness of the Physics Informed Neural Networks (PINNs) for learning the dynamics of constrained Hamiltonian systems is demonstrated using the Dirac theory of constraints for regular systems with holonomic constraints and systems with non-standard Lagrangians. By utilizing Dirac brackets we derive the Hamilton-Dirac equations and we minimize their residual incorporating also energy conservation and the Dirac constraints using appropriate regularization terms in the loss function. The resulting PINNs, referred to as Hamilton-Dirac Neural Networks (HDNNs), successfully learn constrained dynamics without deviating from the constraint manifold. Two examples with holonomic constraints are presented: the simple pendulum in Cartesian coordinates and a two-dimensional elliptically restricted harmonic oscillator. In both cases, HDNNs exhibit superior performance in preserving energy and the constraints compared to traditional explicit solvers. To demonstrate applicability in systems with singular Lagrangians, we computed the guiding center motion in a strong magnetic field starting from the guiding center Lagrangian. The imposition of energy conservation during the neural network training proved essential for accurately determining the orbits of the guiding center.

1 Introduction

The motion of mechanical systems is often restricted by several types of constraints that limit the trajectories within a specific area of the phase space, known as the constraint manifold. When numerically integrating these systems, a common issue arises – the simulated dynamics tend to drift away from the constraint manifold. As a result, the numerical solution becomes inherently inaccurate and unreliable. Addressing this challenge has been a focus for several researchers, and thus many works have been dedicated in the simulation of constrained Hamiltonian systems over the past decades e.g. [1–5]. In these studies constraints arising due to singular Lagrangians or externally imposed holonomic constraints on regular systems, have been taken into account employing the Dirac theory of constraints [6–8], either by using extended Hamiltonians or the Dirac bracket approach. Dirac brackets have also been employed in calculating steady state vortex solutions to fluid equations via a Dirac bracket simulated annealing method [9, 10].

In recent years there has been a surge of interest in developing numerical methods that leverage unsupervised or semi-supervised machine learning to solve initial and boundary value problems. Various neural network architectures are utilized for this purpose, with the most commonly employed being the feed-forward deep neural networks (NNs). This approach is based on the universal approximation theorem of NNs which asserts that an NN with at

*kaltsas.d.a@gmail.com

least one hidden layer can approximate any continuous function with arbitrary accuracy [11]. These networks are trained so that they learn the physical differential equations and the underlying physical laws, and consequently they are referred to as Physics Informed Neural Networks (PINNs) [12–16]. In several works, PINNs are augmented with ground truth data and constraints corresponding to experimental measurements or observations. This allows for the determination of specific parameters in the differential equation, as demonstrated in works such as [12, 17–19]. Additionally, PINNs can be employed to discover the governing differential equations from the provided data, as shown in studies like [20–22]. Among other problems, unsupervised PINNs have also been employed for the integration of integrable and chaotic canonical Hamiltonian systems that conserve the Hamiltonian function [23, 24], following works on data-driven learning of integrable and chaotic Hamiltonian and Lagrangian dynamics [22, 25–29]. In particular, in [23] the authors follow a completely unsupervised machine learning approach to construct neural network solutions to integrable Hamiltonian systems, such as a nonlinear oscillator and the chaotic Hénon-Heiles system, showcasing the remarkable ability of NNs to learn Hamiltonian dynamics without the use of data. In the same work, the single networks are utilized for the entire Hamiltonian system, so the network can adapt to describe underlying interdependencies between the dependent variables. Moreover, the networks are trained not only to satisfy the Hamiltonian equations of motion but also to satisfy energy conservation which is imposed as a regularization term in the total loss function, penalizing violation of this conservation law. This approach ensures that the trained NNs accurately satisfy the equations of motion and the energy conservation, enhancing the network’s accuracy for long-time simulations. Remarkably, the trained networks outperform explicit symplectic integrators in terms of accuracy and energy conservation.

Deep learning and neural network algorithms have also been employed for constrained Hamiltonian systems recently in [30, 31]. In [30] the authors examined the effectiveness of NNs to learn the dynamics of a series of chaotic systems embedded in Cartesian coordinates explicitly imposing the constraints in the Lagrangian, instead of introducing generalized coordinates to encode implicitly the holonomic constraints of these systems. Their approach is data-driven, i.e. the Hamiltonian and the Lagrangian functions are approximated by neural networks which are trained by ground-truth data, while imposing known holonomic constraints. Notably, they found that embedding the system in Cartesian coordinates with explicit constraints leads to a significant improvement in accuracy and data efficiency. It is argued that implicitly imposing holonomic constraints through the use of generalized coordinates can make learning the Hamiltonian and Lagrangian of a system challenging. On the contrary, separating constraints from the Lagrangian and the Hamiltonian may alleviate this difficulty, given the simpler forms these functions assume in Cartesian coordinates. A more recent supervised approach is presented in [31] where stabilized neural differential equations were proposed. In this work, the authors introduce stabilization terms designed to stabilize the dynamics on the constraint manifold, bypassing the need for the Hamiltonian or Lagrangian formalism.

In the present work we revisit the Dirac theory of constraints, reviewing the Dirac’s algorithm to identify primary and secondary constraints [6, 7], the distinction between first-class and second-class constraints and we describe the construction of the Dirac bracket exploiting second-class constraints. The Dirac bracket endows with a new symplectic structure the phase-space and the constraint manifold becomes a Casimir manifold, i.e. the constraints are Casimir functions of the Dirac bracket. By the Dirac bracket and the canonical Hamiltonian of the system the Hamilton-Dirac equations governing the constrained dynamics can be derived. Then we employ a PINN algorithm to simulate the constrained dynamics by computing neural network solutions to the Hamilton-Dirac equations instead of introducing regularization terms in the loss function on the account of the constraints. We term these feed-forward deep neural networks as Hamilton-Dirac NNs (HDNNs). The penalization of the networks by

regularization terms that include the Dirac constraints can only enhance the performance of the algorithm and the accuracy of the neural network solutions. We essentially suggest that the network architecture proposed in [23], which utilizes the outputs of a single network as the canonical variables, resulting in shared internal connectivities among these variables, not only enhances the learning of variable interdependencies more efficiently but also assimilates imposed constraints seamlessly, eliminating the necessity of introducing generalized coordinates. As reported in [30], the introduction of generalized coordinates might be associated with inefficiency in the training of the Hamiltonian or the Lagrangian networks. This work differs from previous studies on this topic by employing an unsupervised methodology, as done in [23]. Furthermore, it exploits the Dirac bracket approach, emphasizing its role in stabilizing the motion on the constraint manifold. Additionally, we apply the same algorithm to address problems with singular Lagrangians that commonly arise in Plasma Physics, such as guiding center motion.

When comparing with traditional numerical algorithms it should be said that, of course, the training of the network requires more computational time. In some instances this time is many orders of magnitude larger than the cpu time of a traditional explicit solver. However, it should be noted that the remarkable conservation properties of the NN solutions can be achieved only with specialized implicit and semi-implicit symplectic integrators, whose implementation though is accompanied with other bottleneck effects such as the solution of nonlinear algebraic systems in each time step, which significantly increase the computational cost. This cost can become prohibitively large for high dimensional problems with a large number of degrees of freedom. For holonomically constrained systems, when it is not trivial or even possible to exploit the holonomic constraints to reduce the dimensionality of the configuration space this problem can be even more pronounced. Neural network algorithms do not suffer from the “curse of dimensionality” [32] and therefore they can become more efficient for high-dimensional problems. In addition, the NN solutions possess the advantage of being closed-form, continuous solutions and no interpolation is required between the discrete points of the computational grid. In addition, if the solutions exhibit some kind of periodicity, the network can be used to adequately describe time intervals beyond the training dataset. This implies that an intermittent training that skips certain time intervals would be possible, reducing the computational time. The ability of the NN algorithms to predict the dynamics in time intervals exempted from the training process can be improved using recurrent network architectures such as the echo state networks. Other promising approaches in enhancing the competitiveness of PINNs over traditional numerical methods in terms of computational time, are the exploitation of parallel computing capabilities for training, which is rather straightforward in the case of NNs and the utilization of transfer learning techniques by utilizing pre-trained networks that fit in the specific physical problem, such as GPT-PINNs [33]. Research in these directions is left for future work.

The rest of the paper is structured as follows: Section 2 provides a brief overview of the Dirac theory of constraints, introducing key concepts such as primary and secondary constraints, first-class and second-class constraints, the Dirac bracket, and the Hamilton-Dirac equations of motion. In Section 3, we present the HDNN algorithm designed for solving constrained Hamiltonian systems. Section 4 presents a series of numerical experiments, demonstrating the effectiveness of the HDNN approach in simulating Hamiltonian systems with holonomic constraints. Additionally, an example featuring a system with a singular Lagrangian is included. Finally, we summarize our findings in Section 5

2 Constrained Hamiltonian systems and Dirac brackets

2.1 Hamiltonian mechanics

In this section, we briefly review the canonical Hamiltonian dynamics and the Dirac theory of constraints (e.g. see [3]). Central to the canonical Hamiltonian description of a finite degree-of-freedom Hamiltonian system is the canonical Hamiltonian function defined through a Legendre transformation:

$$H_c = \dot{q}^i p_i - L(q, \dot{q}), \quad (1)$$

where q^i , $i = 1, \dots, N$, are the canonical coordinates, $L(q, \dot{q})$ is the Lagrangian function and

$$p_i = \frac{\partial L}{\partial \dot{q}^i}, \quad i = 1, \dots, N, \quad (2)$$

are the conjugate momenta. We can introduce a phase-space vector $\mathbf{z} = (q^1, \dots, q^N, p_1, \dots, p_N)$ to describe the dynamics in the phase space, determined by the Hamiltonian function and the Poisson bracket, given by:

$$\{F, G\} = \frac{\partial F}{\partial q^i} \frac{\partial G}{\partial p_i} - \frac{\partial G}{\partial q^i} \frac{\partial F}{\partial p_i} = \frac{\partial F}{\partial z^i} \mathcal{J}_c^{ij} \frac{\partial G}{\partial z^j}, \quad (3)$$

where $F(\mathbf{z})$, $G(\mathbf{z})$ are two phase space functions and \mathcal{J}_c is the canonical Poisson operator defined as:

$$\mathcal{J}_c = \begin{pmatrix} 0_N & I_N \\ -I_N & 0_N \end{pmatrix}, \quad (4)$$

with 0_n and I_n being the n -dimensional zero and identity matrices, respectively.

The Poisson bracket endows the phase space the structure of a symplectic manifold and together with the canonical Hamiltonian (1) determine the dynamics through the Hamilton's equations:

$$\dot{z}^i = \{z^i, H_c\} = \mathcal{J}_c^{ij} \frac{\partial H_c}{\partial z^j}. \quad (5)$$

As \mathcal{J}_c is an antisymmetric matrix, the time derivative of the constrained Hamiltonian, is $dH_c/dt = H_c$, $H_c = 0$. Consequently, the Hamiltonian H_c is a constant of motion. Moreover, from a geometric perspective, the symplectic volume form (phase-space volume) is preserved under the Hamiltonian flow determined by the Hamiltonian function and the above Poisson structure.

2.2 Non-standard Lagrangians and Dirac constraints

For non-standard Lagrangians where the Hessian $\partial^2 L / \partial \dot{z}^i \partial \dot{z}^j$ is singular, some of the equations (2) cannot be used to solve for the corresponding \dot{q}^i 's, instead yielding relations of the form:

$$\Phi_\alpha(\mathbf{z}) = 0, \quad \alpha = 1, \dots, K \leq N, \quad (6)$$

which are called primary constraints that define the constraint manifold. On this manifold the total Hamiltonian

$$H_t = H_c + \zeta^\alpha \Phi_\alpha, \quad (7)$$

where ζ^α can be a function of q 's and p 's, should produce the same dynamics as H_c . Substituting (7) into Hamilton's equations (5) leads to

$$\dot{z}^i = \{z^i, H_t\} = \mathcal{J}_c^{ij} \frac{\partial H_c}{\partial z^j} + \zeta^\alpha \mathcal{J}_c^{ij} \frac{\partial \Phi_\alpha}{\partial z^j}, \quad (8)$$

which hold true on the constraint manifold: $\Phi_\alpha = 0, \forall \alpha$, i.e. it differs from the ordinary Hamiltonian system $\dot{z}^i = \{z^i, H_t\}$, only by a linear combination of the constraint functions Φ_κ .

The dynamics of the system should comply with the constraints and therefore the latter should be preserved by the dynamics. Hence, in a consistent description we should have

$$\dot{\Phi}_\alpha = \{\Phi_\alpha, H_t\} \approx 0, \quad (9)$$

where \approx is a weak equality, i.e. it holds true after the constraints are taken into account. Equation (9) can generally lead us to a new set of equations of the form:

$$\Psi_\beta(\mathbf{z}) = 0, \quad \beta = 1, \dots, M \leq K. \quad (10)$$

Equations (10) can be either used to determine the multipliers ζ^α or, in cases where this is not possible, they are seen as secondary constraints, which should be preserved by the dynamics as well. The Dirac algorithm [6, 7] dictates that the consistency requirement (9) should be applied also to the secondary constraint functions ψ_β until we have determined all primary and secondary constraints.

Let us examine an example where Eqs. (10) can either be used to determine the multipliers ζ^α or can also lead to tertiary constraints, considering the Lagrangian

$$L = \dot{q}^i G_i(q, t) - W(q), \quad i = 1, \dots, N, \quad (11)$$

which emerges in the context of energetically consistent guiding center theories describing the motion of charged particle guiding centers in strong magnetic fields while satisfying fundamental conservation laws (e.g. see [34–37]). The conjugate momenta corresponding to the lagrangian (11) are

$$p_i = \frac{\partial L}{\partial \dot{q}^i} = G_i(q), \quad (12)$$

thus we have the following primary constraints:

$$\Phi_k = p_k - G_k(q) = 0, \quad k = 1, \dots, N \quad (13)$$

and the total Hamiltonian is given by

$$H_t = \dot{q}^i p_i - L + \zeta^k [p_k - G_k(q)] = W(q) + \zeta^k [p_k - G_k(q)]. \quad (14)$$

Following Dirac's algorithm we check whether the primary constraints are preserved by the dynamics

$$\dot{\Phi}_k = \{\Phi_k, H_t\} \approx -\frac{\partial G_k}{\partial q^i} \zeta^i - \left(\frac{\partial W}{\partial q^i} - \zeta^j \frac{\partial G_j}{\partial q^i} \right) \delta^{ik} = -\frac{\partial W}{\partial q^k} - \left(\zeta^i \frac{\partial G_k}{\partial q^i} - \zeta^j \frac{\partial G_j}{\partial q^k} \right), \quad (15)$$

Then, the equations

$$\Psi_k = -\frac{\partial W}{\partial q^k} - \left(\zeta^i \frac{\partial G_k}{\partial q^i} - \zeta^j \frac{\partial G_j}{\partial q^k} \right) = -\frac{\partial W}{\partial q^k} - \mathcal{Z}_{ik} \zeta^i \approx 0, \quad i, k = 1, \dots, N, \quad (16)$$

can be used to uniquely determine the multipliers ζ^k if $\det(\mathcal{Z}) \neq 0$, thus concluding the Dirac's algorithm. On the other hand, if the system is not solvable, we end up with a set of secondary constraints. For example, let us consider the case where the second term in (16) vanishes for some ℓ , hence, we end up with a secondary constraint of the form:

$$\Psi_\ell = -\frac{\partial W}{\partial q^\ell}, \quad (17)$$

and we have to check its conservation:

$$\dot{\Psi}_\ell = \{\Psi_\ell, H_t\} = -\zeta^k \frac{\partial^2 W}{\partial q^\ell \partial q^k} = -\sum_{m \neq \ell} \zeta^m \frac{\partial^2 W}{\partial q^m \partial q^\ell} - \zeta^\ell \frac{\partial^2 W}{\partial q^\ell \partial q^\ell} \approx 0. \quad (18)$$

If $\partial^2 W / \partial q^\ell \partial q^\ell \neq 0$ we have an equation that determines the multiplier ζ^ℓ :

$$\zeta^\ell = -\frac{1}{\partial^2 W / \partial q^\ell \partial q^\ell} \sum_{m \neq \ell} \zeta^m \frac{\partial^2 W}{\partial q^m \partial q^\ell}, \quad (19)$$

and the algorithm stops here.

2.3 The Dirac bracket

After identifying all primary and secondary constraints using the Dirac algorithm, we can further classify them into first class and second class constraints. Denoting all constraint functions, including primary and secondary, as χ_α for $\alpha = 1, \dots, A$, we define second class constraints as those for which the matrix C of their Poisson brackets:

$$C_{\alpha\beta} = \{\chi_\alpha, \chi_\beta\}, \quad (20)$$

is regular and thus can be inverted, while first class constraints do not satisfy this condition as their Poisson bracket with all other constraints vanishes weakly $\{\chi_\alpha, \chi_\beta\} \approx 0$. First class constraints are associated with gauge symmetries of the Lagrangian while second class constraints are associated with redundant degrees of freedom. By introducing the Dirac bracket [38], the second class constraints become Casimir invariants of the Dirac bracket [3]. In the subsequent analysis we consider cases with second class constraints only, so that the matrix (20) is invertible, and the following generalized Poisson bracket between two phase-space functions F, G can be defined

$$\{F, G\}_* = \{F, G\} - \{F, \chi_\alpha\} (C^{-1})^{\alpha\beta} \{\chi_\beta, G\}. \quad (21)$$

The bracket $\{F, G\}_*$ is referred to as the Dirac bracket, possessing the same algebraic properties as the ordinary Poisson bracket. As such, it also imparts a symplectic structure to the phase space. It can be easily shown [3] that

$$\{F, H_c\}_* \approx \{F, H_t\}, \quad (22)$$

that is the two brackets generate identical dynamics on the constraint manifold. Therefore, Hamilton's equations (8) can be replaced by the equations

$$\dot{z}^i = \{z^i, H_c\}_* = \{z^i, H_c\} - \{z^i, \chi_\alpha\} (C^{-1})^{\alpha\beta} \{\chi_\beta, H_c\},$$

or

$$\dot{z}^i = \mathcal{J}_c^{ij} \frac{\partial H_c}{\partial z^j} - \mathcal{J}_c^{ij} \frac{\partial \chi_\alpha}{\partial z^j} (C^{-1})^{\alpha\beta} \{\chi_\beta, H_c\}, \quad (23)$$

called the Hamilton-Dirac equations. The second term in the rhs of (23) can be interpreted as generalized forces that impose the constraints in the dynamics. Also notice that (23) can be written as

$$\dot{z}^i = \left[\delta_k^i - \mathcal{J}_c^{ij} \frac{\partial \chi_\alpha}{\partial z^j} (C^{-1})^{\alpha\beta} \frac{\partial \chi_\beta}{\partial z^k} \right] \mathcal{J}_c^{kl} \frac{\partial H_c}{\partial z^\ell} = \mathcal{P}_k^i \mathcal{J}_c^{kl} \frac{\partial H_c}{\partial z^\ell}, \quad (24)$$

where $\mathcal{P} = I - \mathcal{J}_c \cdot (\nabla_z \chi_\alpha) (C^{-1})^{\alpha\beta} (\nabla_z \chi_\beta)$ is a projection operator. Therefore the constrained dynamics can be interpreted as projections of the original dynamics on the constrained manifold.

With this formulation it is straightforward to show that the constraint functions χ_α , $\forall \alpha$ are preserved by the dynamics, as they are in fact, Casimir invariants of the Dirac bracket, i.e. they Dirac-commute with any phase space function $F(z)$:

$$\{\chi_\alpha, F\}_* = \{\chi_\alpha, F\} - \{\chi_\alpha, \chi_\beta\} (C^{-1})^{\beta\gamma} \{\chi_\gamma, F\} = 0, \quad \forall F. \quad (25)$$

As a final theory note we mention that one can retrieve the Hamilton-Dirac equations (23) without introducing the Dirac bracket (21) but by constructing an extended Hamiltonian function

$$H_e = H_c + \zeta^\alpha \chi_\alpha, \quad (26)$$

where χ_α are all the constraints of the system, primary and secondary. Then one can show [3] that the multipliers ζ^α can be computed by the consistency requirement $\{\zeta^i, H_e\} \approx 0$ resulting in

$$\zeta^\alpha = -(C^{-1})^{\alpha\beta} \{\chi_\beta, H_e\}, \quad (27)$$

and

$$\{z^i, H_e\} \approx \{z^i, H_c\}_*, \quad i = 1, \dots, 2N, \quad (28)$$

as shown in [1]. Notice that in view of (28) the equations of motion produced by the extended Hamiltonian (26) and the ordinary Poisson bracket are weakly but not strongly equivalent to the Hamilton-Dirac equations (23).

2.4 Regular systems with holonomic constraints

We started the presentation of the Dirac theory of constraints assuming that they arise due to singular, non-standard Lagrangians. However, the methodology presented above can be employed in order to impose holonomic constraints of the form $\Phi_\alpha(q) = 0$ to a system with a regular Lagrangian L . Again, one can define the total Hamiltonian $H_t = H_c + \zeta^\alpha \Phi_\alpha$ and see Φ_α as primary constraints. Then the consistency condition $\dot{\Phi}_\alpha = 0$ leads to secondary constraints Ψ_β . The multipliers ζ^α can be determined by imposing the consistency condition to the secondary constraints, leading to

$$\{\Psi_\beta, H_c\} + \zeta^\alpha \{\Psi_\beta, \Phi_\alpha\} \approx 0, \quad (29)$$

which can be solved for ζ^α as follows

$$\zeta^\alpha \approx -(C^{-1})^{\alpha\beta} \{\Psi_\beta, H_c\} = -(C^{-1})^{\alpha\beta} \frac{\partial \Psi_\beta}{\partial z^i} \mathcal{J}_c^{ij} \frac{\partial H_c}{\partial z^j}. \quad (30)$$

A standard approach (see [3]) is then to use the Hamilton equations substituting the total Hamiltonian with multipliers ζ^α determined by Eqs. (30). Hence, after taking into account the constraints we have equations (8) with multipliers (30), i.e.

$$\dot{z}^i = \left[\delta_k^i - \mathcal{J}_c^{ij} \frac{\partial \Phi_\alpha}{\partial z^j} (C^{-1})^{\alpha\beta} \frac{\partial \Psi_\beta}{\partial z^k} \right] \mathcal{J}_c^{kl} \frac{\partial H_c}{\partial z^\ell}. \quad (31)$$

Alternatively, we can construct the Dirac bracket or define the extended Hamiltonian and use the standard Poisson bracket as shown in the previous section. All formalisms are weakly equivalent, i.e. the equations of motion obtained by the three formulations are identical after imposing the constraints, but there might be significant differences regarding the stabilization of the phase space trajectories on the constraint manifold or the computational cost as shown in [3].

3 Approximating constrained dynamics with PINNs

The $2N$ canonical dynamical variables z^i , $i = 1, \dots, 2N$ are approximated by a single feed forward, fully connected, deep neural network with $2N$ output neurons Z_{net}^i , each corresponding to one variable and one input neuron that corresponds to the time variable t . The initial conditions

$$z^i(t_0) = z_0^i, \quad i = 1, \dots, 2N, \quad (32)$$

can be imposed either in the training process by penalizing the network when violating the initial conditions or it can be imposed as a hard-constraint by constructing solutions of the form:

$$z^i(t) = z_0^i + f(t)Z_{net}^i(t), \quad i = 1, \dots, 2N, \quad (33)$$

where $f(t)$ is appropriately selected so that $f(t_0) = 0$ and $Z_{net}^i(t)$ are the outputs of a feed-forward fully-connected deep neural network. In [23] the authors selected $f(t) = 1 - e^{-t}$ and $f(t) = t$, with the second having the disadvantage of being unbounded from above. Alternatives, can be $f(t) = \tanh(t)$ and $f(t) = \sigma(t) = 1/(1 + e^{-t})$. In this study we use $f(t) = 1 - e^{-\gamma t}$ where γ can be a learnable parameter.

The independent variable t is discretized so as the constrained dynamics is evaluated on a set $\mathcal{T} = (t_1, \dots, t_n)$ of n discrete time points. Consequently we form the following loss function

$$\mathcal{L} = \frac{1}{n} \sum_{i=1}^{2N} \sum_{t \in \mathcal{T}} \left| \dot{z}^i(t) - \mathcal{J}_c^{ij} \frac{\partial H_c}{\partial z^j} + \mathcal{J}_c^{ij} \frac{\partial \chi_\alpha}{\partial z^j} (C^{-1})^{\alpha\beta} \{\chi_\beta, H_c\} \right|^2 + L_{reg}, \quad (34)$$

where

$$\mathcal{L}_{reg} = w_{en} \mathcal{L}_{en} + w_c \mathcal{L}_c, \quad (35)$$

with w_{en} and w_c being weight parameters and

$$\mathcal{L}_{en} = \frac{1}{n} \sum_{t \in \mathcal{T}} \left| H_t(\mathbf{z}(t)) - H_{t_0} \right|^2, \quad (36)$$

$$\mathcal{L}_c = \frac{1}{n} \sum_{\alpha=1}^{K+M} \sum_{t \in \mathcal{T}} \left| \chi_\alpha(\mathbf{z}(t)) \right|^2, \quad (37)$$

are two regularization terms which penalize the network whenever the dynamics do not satisfy, respectively, the conservation of the total Hamiltonian and the Dirac constraints, both primary and secondary. Evidently, the quantity $H_{t_0} = H_t(\mathbf{z}_0)$ is the initial value of the total Hamiltonian.

The internal parameters \mathbf{p}_{net} of the neural network are trained so that the above loss function is minimized, i.e. the training of the HDNN amounts to the optimization problem

$$\arg \min_{\mathbf{p}_{net}} \mathcal{L}, \quad (38)$$

with \mathcal{L} given by (34). The time derivative in (34) is computed using the PyTorch automatic differentiation engine that utilizes the backpropagation algorithm. The discretization method of the variable t is the same with the method described in [23] which utilizes stochastic perturbation of the grid points in each training epoch. One can use different activation functions for the neurons of the HDNN, e.g. the sigmoid, tanh, SiLU, $\sin(x)$ are common candidates. For systems exhibiting periodic motions, the most natural choice is a trigonometric activation function, i.e. $\sin(\delta x)$ with δ being a learnable parameter.

4 Experiments

4.1 Regular Lagrangians and holonomic constraints: planar pendulume in cartesian coordinates

Let us consider a simple pendulum described in Cartesian coordinates (x, y, z) , moving in a gravitational acceleration field $\mathbf{g} = -g\hat{y}$ and restricted to the plane (x, y) at a constant distance ℓ from the origin $(0, 0)$. The Lagrangian is given by:

$$L = \frac{m}{2}(\dot{x}^2 + \dot{y}^2) - mgy, \quad (39)$$

and the primary constraint is

$$\Phi = \frac{1}{2}(x^2 + y^2 - \ell^2), \quad (40)$$

where $\ell^2 = x_0^2 + y_0^2$. The canonically conjugate momenta, the canonical and the total Hamiltonian functions are, respectively

$$p_x = \frac{\partial L}{\partial \dot{x}} = m\dot{x}, \quad p_y = \frac{\partial L}{\partial \dot{y}} = m\dot{y}, \quad (41)$$

$$H_c = \frac{1}{2m}(p_x^2 + p_y^2) + mgy, \quad (42)$$

$$H_t = \frac{1}{2m}(p_x^2 + p_y^2) + mgy - \frac{\lambda}{2}(x^2 + y^2 - \ell^2), \quad (43)$$

where λ is a Lagrangian multiplier. The primary constraint (40) should be preserved by the dynamics, thus

$$\{\Phi, H_t\} = m^{-1}(xp_x + yp_y) \approx 0, \quad (44)$$

that leads to the secondary constraint

$$\Psi = xp_x + yp_y, \quad (45)$$

which is a Pfaffian constraint [39]. Demanding the weak conservation of Ψ we find an explicit relation for the multiplier λ :

$$\lambda = \frac{1}{x^2 + y^2} \left(mgy - \frac{p_x^2 + p_y^2}{m} \right), \quad (46)$$

and thus the Dirac algorithm concludes at this point with the identification of the constraints Φ and Ψ . We can now define the matrix C as follows

$$C = \begin{pmatrix} \{\Phi, \Phi\} & \{\Phi, \Psi\} \\ \{\Psi, \Phi\} & \{\Psi, \Psi\} \end{pmatrix} = \begin{pmatrix} 0 & x^2 + y^2 \\ -x^2 - y^2 & 0 \end{pmatrix}, \quad (47)$$

whose inverse is

$$C^{-1} = \begin{pmatrix} 0 & -\frac{1}{x^2 + y^2} \\ \frac{1}{x^2 + y^2} & 0 \end{pmatrix}. \quad (48)$$

Knowing the matrix C^{-1} we can construct the corresponding Dirac bracket between two phase-space functions F and G using (21)

$$\{F, G\}_* = \{F, G\} - \frac{1}{x^2 + y^2} (\{F, \Psi\}\{\Phi, G\} - \{F, \Phi\}\{\Psi, G\}). \quad (49)$$

Consequently, the Hamilton-Dirac equations of motion are

$$\dot{x} = \{x, H_c\}_* = \frac{p_x}{m} + \mu x, \quad (50)$$

$$\dot{y} = \{y, H_c\}_* = \frac{p_y}{m} + \mu y, \quad (51)$$

$$\dot{p}_x = \{p_x, H_c\}_* = \lambda x - \mu p_x, \quad (52)$$

$$\dot{p}_y = \{p_y, H_c\}_* = \lambda y - \mu p_y - mg, \quad (53)$$

where

$$\mu = -\frac{xp_x + yp_y}{m(x^2 + y^2)}. \quad (54)$$

An alternative to the Dirac bracket approach is the use of the ordinary Poisson bracket along with the extended Hamiltonian, which is composed by the canonical Hamiltonian plus the linear combination of the constraints Φ and Ψ with multipliers ζ determined by (27). The resulting equations are weakly identical to equations (50)–(53), meaning they reduce to those equations after applying the constraints, as indicated by equation (28). Another standard approach involves using the total Hamiltonian (43) substituted into the standard Hamilton equations with λ given by equation (46) (which can be calculated from equation (30)). In [38], it was demonstrated that among these three approaches, the Dirac bracket and the extended Hamiltonian methods are the more accurate, yielding similar results. However, the Dirac bracket approach is less computationally expensive. Prompted by this observation, we employ here only the Dirac bracket approach, which is enhanced though by the imposition of two additional regularization terms in the loss function that is minimized during the HDNN training.

The total loss function is given by (34) with $\mathbf{z}(t) = (x(t), y(t), p_x(t), p_y(t))$ and the Hamilton-Dirac equation residual in the first term of (34) is determined by Eqs. (50)–(53). The regularization term is constructed using the total Hamiltonian (43) and the constraints (40) and (45). In Fig. 1 we plotted the time series for x, y, p_x, p_y obtained by the neural network solution (33) versus the “exact solution” determined by solving the Hamilton-Dirac equations with the LSODA¹ algorithm using a dense grid. For assessing the constrained neural network method we also integrated Eqs. (50)–(53) using the fifth order Runge-Kutta (RK45) method. It is evident that the HDNN solution conserves the amplitude of the oscillation in all variables, and consequently the energy is conserved, in contrast to the RK45 method which exhibits dissipation.

The energy conserving property of the simple pendulum HDNN is also corroborated by plotting the normalized energy difference $(E(t) - E_0)/E_0$ versus time for the HDNN solution contrasted to the numerical solution obtained by RK45 in Fig. 2. We also plot the pendulum trajectory in various sections of the phase-space. For the sake of illustration we present the trajectories on the planes $x - y$, $x - p_x$ and $p_x - p_y$ in Fig. 3. For this particular example we have performed a numerical evaluation over a time domain $[0, 20T]$ where T is the period of the nonlinear pendulum and we have used a NN architecture with 4 hidden layers and 80 neurons per layer. The network has been trained for 10000 training epochs using 2000 discrete time points in the $[0, 20T]$ time domain. Regarding the performance of the NN algorithm, the training time was 5.09 minutes on an Nvidia RTX-3060 GPU whereas the RK45 solver took 0.015 secs using the same time resolution. Clearly, the training of the NNs is far from efficient in terms of computational time. Nevertheless, as mentioned in the introduction, NN methods can be significantly accelerated using parallel computing, pre-trained networks, and training strategies involving leap time intervals.

Finally, to assess the importance of imposing Dirac constraints in the regularization term (34), we plot the history of its different components. The first term quantifies the residual of

¹LSODA is an Adams/BDF numerical method with automatic stiffness detection and automatic switching.

the equations of motion, while the two terms comprising \mathcal{L}_{reg} in (35) quantify the energy drift and the violation of Dirac constraints. In Fig. 4, we compare the loss history for a HDNN with constraints (40) and (45) explicitly imposed in \mathcal{L}_{reg} with the corresponding loss history without imposing the constraints. It is evident that explicitly imposing the constraints not only helps the network learn the trajectory by respecting the constraints, but also facilitates energy conservation and minimizes the residual of the equations.

4.2 Elliptically restricted 2D harmonic oscillator

The real advantage of the Dirac method becomes evident when considering its applicability to every holonomic constraint expressed in the form $f(q_1, \dots, q_N) = 0$. In many cases, there is no suitable coordinate system available to effectively reduce the dimensionality of the problem. In this subsection, we will consider the case of an elliptically restricted 2D harmonic oscillator, wherein a mass $m = 1$ moves within a potential of the form

$$V(x, y) = \frac{\alpha}{2}x^2 + \frac{\beta}{2}y^2, \quad (55)$$

and its motion is constrained on the ellipse

$$x^2 + \frac{y^2}{1 - \epsilon^2} - a^2 = 0, \quad (56)$$

where a is the semi-major axis and ϵ is the eccentricity of the ellipse.

Of course, one could use elliptic coordinates to study this problem, however, such an analysis would be more cumbersome. Furthermore, it is worth reiterating that the Dirac method can be applied to restrict the motion on any shape defined by $f(x, y) = 0$, making it more general. The problem considered in this subsection truly underscores the advantage of the HDNNs over traditional numerical solvers as it will become evident that both the LSODA and RK45 methods struggle to restrict motion on the constrained manifold, even with a very dense time grid. In contrast, the orbits of the HDNN solutions remain on the constraint manifold for long time simulations.

In this particular example the primary constraint function is

$$\Phi(x, y) = \frac{1}{2} \left(x^2 + \frac{y^2}{1 - \epsilon^2} - a^2 \right). \quad (57)$$

Repeating the analysis of the previous subsection, we find the following secondary Pfaffian constraint and total Hamiltonian:

$$\Psi = xp_x + \frac{yp_y}{1 - \epsilon^2}, \quad (58)$$

$$H_t = \frac{p_x^2}{2} + \frac{p_y^2}{2} + V(x, y) - \frac{\lambda}{2} \left(x^2 + \frac{y^2}{1 - \epsilon^2} - a^2 \right), \quad (59)$$

where

$$\lambda = \frac{p_x^2 + \frac{p_y^2}{1 - \epsilon^2} - \alpha x^2 - \frac{\beta y^2}{1 - \epsilon^2}}{x^2 + \frac{y^2}{(1 - \epsilon^2)^2}}, \quad (60)$$

is the Lagrange multiplier determined by the consistency condition $\{\Psi, H_t\} = 0$. The Dirac bracket is

$$\{F, G\}_* = \{F, G\} - \frac{1}{x^2 + \frac{y^2}{(1 - \epsilon^2)^2}} (\{F, \Psi\}\{\Phi, G\} - \{F, \Phi\}\{\Psi, G\}), \quad (61)$$

and the Hamilton-Dirac equations of motion read as follows:

$$\dot{x} = \{x, H_c\}_* = p_x + \mu x, \quad (62)$$

$$\dot{y} = \{y, H_c\}_* = p_y + \mu y \quad (63)$$

$$\dot{p}_x = \{p_x, H_c\}_* = -\alpha x - \mu p_x - \lambda x, \quad (64)$$

$$\dot{p}_y = \{p_y, H_c\}_* = -\beta x - \mu p_y - \lambda y, \quad (65)$$

where

$$\mu = -\frac{x p_x + \frac{y p_y}{1-\epsilon^2}}{x^2 + \frac{y^2}{(1-\epsilon^2)^2}}. \quad (66)$$

We train a HDNN so that (33) satisfies Eqs. (62)–(65), while it preserves the constraint functions Φ , Ψ and the total Hamiltonian H_t (Eqs. (57), (58) and (59), respectively) by minimizing the loss function as defined in Eq. (34). We perform this minimization and additionally we solve the system (62)–(65) with the RK45 method and the LSODA algorithm, with initial conditions are $(x_0, y_0, p_{x0}, p_{y0}) = (0.5, 0.5, 0.2, 0.0)$ and potential function parameters $\alpha = 0.1$, $\beta = 0.4$. For this particular choice of parameters the unrestricted motion is in 1 : 2 resonance and has a figure-8 trajectory on the $x - y$ plane (see Fig. 6). The eccentricity of the elliptical constraint (57) is $\epsilon = 0.2$. The HDNN solution was trained in the time domain $[0, 360]$ using 500 grid points which are stochastically perturbed in each training epoch while for the standard numerical methods we used a grid with 5000 points. In the training procedure we employed transfer learning to enhance efficiency. Initially, the network underwent training for 10000 epochs within the domain $[0, 50]$. Subsequently, we gradually extended the domain by 50 time units until reaching $[0, 350]$. After each extension, the network underwent another 10,000 epoch training period, totaling 7 training periods with 10000 epochs each. The entire training process lasted 5.75 minutes.

In Fig. 5, we compare the HDNN solution with the numerical solutions obtained using LSODA and RK45 methods. The latter solutions exhibit unphysical behavior, while the HDNN solution remains stable, satisfying energy conservation and preserving Dirac constraints. This is evident from the trajectories in Fig. 6, the energy drift time series in Fig. 7, and the time evolution of the constraint functions in Fig. 8. Despite the lower computational efficiency of the training procedure compared to explicit numerical methods, this example demonstrates the superiority of an HDNN algorithm over traditional numerical solvers for specific problems, such as the constrained motion on non-trivial curves. Moreover, it highlights the potential for leveraging NN algorithms in the study of classical circularly and elliptically restricted many body problems.

4.3 Singular Lagrangians: guiding center motion

In this subsection we study the motion of a guiding center in a strong magnetic field of constant direction. Following the normalization of [40], the Lagrangian for the guiding center motion [34] is given by

$$L(\mathbf{x}, \dot{\mathbf{x}}, u_{\parallel}, \dot{u}_{\parallel}) = [\mathbf{A}(\mathbf{x}) + u_{\parallel} \mathbf{b}(\mathbf{x})] \cdot \dot{\mathbf{x}} - W(\mathbf{x}, u_{\parallel}), \quad (67)$$

where the potential function $W(\mathbf{x}, u_{\parallel})$ is

$$W(\mathbf{x}, u_{\parallel}) = \mu |\mathbf{B}(\mathbf{x})| + \frac{u_{\parallel}^2}{2} + \phi(\mathbf{x}). \quad (68)$$

Here, μ is the conserved magnetic moment, $\phi(\mathbf{x})$ is the electrostatic potential and $\mathbf{A}(\mathbf{x})$ is the vector potential, while $\mathbf{b}(\mathbf{x})$ is the unit vector along the magnetic field direction. This is a

typical example of non-standard, singular Lagrangian where the Dirac method of constraints applies and a Dirac bracket can be derived. Without referring to the Dirac method for the construction of a generalized Hamiltonian system the guiding-center equations of motion can be derived by invoking the Euler-Lagrange equations yielding:

$$\dot{\mathbf{x}} = \frac{u_{\parallel} \mathbf{B}^* - \mathbf{b} \times \mathbf{E}^*}{\mathbf{b} \cdot \mathbf{B}^*}, \quad (69)$$

$$\dot{u}_{\parallel} = \frac{\mathbf{B}^* \cdot \mathbf{E}^*}{\mathbf{b} \cdot \mathbf{B}^*}, \quad (70)$$

where

$$\mathbf{A}^* = \mathbf{A} + u_{\parallel} \mathbf{b}, \quad (71)$$

$$\mathbf{E}^* = \mathbf{E} - \mu \nabla |\mathbf{B}|, \quad (72)$$

$$\mathbf{B}^* = \nabla \times \mathbf{A}^*, \quad (73)$$

Several papers have addressed the topic of structure-preserving discretization of these equations so that the conservation properties of the system are retained on the discrete level. However, since the guiding-center Lagrangian is a non-standard Lagrangian, conventional symplectic integration approaches cannot be directly applied. As a result, several authors have turned to the method of Variational Integrators [41] to construct symplectic algorithms capable of preserving conservation properties, making them suitable for long-time simulations of guiding center motion (e.g., [40, 42, 43]). On the other hand though, the guiding center motion is an ideal exemplary for applying the Dirac theory of constraints as demonstrated in [44]. Here, we use the Dirac theory to construct the Dirac bracket and simulate the dynamics of a guiding center with PINNs for the following toy model for a magnetic field

$$\mathbf{B} = \left[1 + \epsilon \left(\frac{x^2}{\kappa} + y^2 \right) \right] \hat{z}, \quad (74)$$

assuming that $\phi(\mathbf{x}) = 0$ as in [40]. In this case the equations of motion (69)–(70) become

$$\dot{x} = -\frac{\mu}{B(x,y)} \frac{\partial B}{\partial y}, \quad (75)$$

$$\dot{y} = \frac{\mu}{B(x,y)} \frac{\partial B}{\partial x}, \quad (76)$$

$$\dot{u}_{\parallel} = 0, \quad (77)$$

and the guiding center motion has an exact closed elliptic orbit.

We can directly integrate these equations with standard numerical methods such as the symplectic Euler method or the 4th order Runge-Kutta (RK4) to achieve higher accuracy. However, for long time simulations the discretization error these methods piles up resulting in a significant drift of the simulated trajectory away of the actual guiding center trajectory. To remedy this problem various variational symplectic integrator approaches have been introduced [40–42] which preserve a noncanonical symplectic structure. These, integrators though, are implicit and nonlinear solvers have to be employed in order to solve the resulting system of equations after discretization. In contrast, symplectic algorithms for canonical Hamiltonian systems can be designed to be explicit and thus significantly less consuming in terms of computational resources and time. Here, we propose an alternative method that utilizes deep neural networks to solve the equations of motion (75)–(77). This can be achieved directly without employing the Dirac method of constraints to construct the total Hamiltonian, by imposing only energy conservation as a regularization term. Here, we utilize the Dirac method to employ the same HDNN architecture as in the previous examples, incorporating

constraints and the total Hamiltonian in the regularization term of the loss function. In both cases, the network successfully learns the guiding center dynamics, outperforming traditional ODE solvers in terms of accuracy, with the same or significantly fewer discretization points in time t . However, the computational time required for network training is significantly longer. This trade-off can be improved on the side of the deep learning approach by utilizing more advanced strategies within the context of equation-driven machine learning.

The Dirac method of constraints is relevant in the context of the guiding center motion since the Lagrangian (11) is linear in the velocities \dot{x} , and \dot{z} and \dot{y} , while \dot{u}_{\parallel} does not appear at all. Therefore, the equations for the corresponding conjugate momenta are

$$p_x = \frac{\partial L}{\partial \dot{x}} = A_x, \quad (78)$$

$$p_y = \frac{\partial L}{\partial \dot{y}} = A_y, \quad (79)$$

$$p_z = \frac{\partial L}{\partial \dot{z}} = A_z, \quad (80)$$

$$p_{u_{\parallel}} = \frac{\partial L}{\partial \dot{u}_{\parallel}} = 0, \quad (81)$$

which are essentially four phase-space constraints as they cannot be solved for the velocities. The constraint functions are $\Phi_1 = p_x - A_x = 0$, $\Phi_2 = p_y - A_y = 0$, $\Phi_3 = p_z - A_z = 0$ and $\Phi_4 = p_{u_{\parallel}} = 0$, while the canonical and the total Hamiltonian are given, respectively, by

$$H_c = \dot{x} \frac{\partial L}{\partial \dot{x}} + \dot{y} \frac{\partial L}{\partial \dot{y}} + \dot{z} \frac{\partial L}{\partial \dot{z}} - L = W(x, y, z, u_{\parallel}), \quad (82)$$

$$H_t = W(x, y, z, u_{\parallel}) + \sum_{\alpha=1}^4 \lambda_{\alpha} \Phi_{\alpha}, \quad (83)$$

where λ_{α} , $\alpha = 1, 2, 3, 4$ are Lagrangian multipliers. By employing the consistency conditions

$$\{\Phi_{\alpha}, H_t\} \approx 0, \quad \alpha = 1, \dots, 4, \quad (84)$$

we can determine the multipliers λ_i :

$$\lambda_1 = -\frac{1}{B(x, y)} \frac{\partial W}{\partial y}, \quad (85)$$

$$\lambda_2 = \frac{1}{B(x, y)} \frac{\partial W}{\partial x}, \quad (86)$$

$$\lambda_3 = u_{\parallel}, \quad \lambda_4 = 0, \quad (87)$$

thus, the total Hamiltonian reads:

$$H_t = W(x, y) - \frac{(p_x - A_x)}{B(x, y)} \frac{\partial W}{\partial y} + \frac{(p_y - A_y)}{B(x, y)} \frac{\partial W}{\partial x} + u_{\parallel}(p_z - A_z). \quad (88)$$

By employing the Dirac approach we essentially embed the dynamical system into the higher-dimensional phase-space. The motion on the $x - y$ plane can be decoupled from the uniform parallel dynamics and thus the non-trivial dynamical equations are

$$\dot{x} = \frac{\partial H_c}{\partial p_x} - \lambda_1 \frac{\partial \Phi_1}{\partial p_x} = -\frac{\mu}{B} \frac{\partial B}{\partial y}, \quad (89)$$

$$\dot{y} = \frac{\partial H_c}{\partial p_y} - \lambda_2 \frac{\partial \Phi_1}{\partial p_y} = \frac{\mu}{B} \frac{\partial B}{\partial x}, \quad (90)$$

$$\dot{p}_x = -\frac{\partial H_c}{\partial x} + \lambda_1 \frac{\partial \Phi_1}{\partial x} = -\frac{\mu}{2} \frac{\partial B}{\partial x} + \frac{\epsilon \mu x y}{\kappa B} \frac{\partial B}{\partial y}, \quad (91)$$

$$\dot{p}_y = -\frac{\partial H_c}{\partial y} + \lambda_2 \frac{\partial \Phi_2}{\partial y} = -\frac{\mu}{2} \frac{\partial B}{\partial y} + \frac{\epsilon \mu x y}{\kappa B} \frac{\partial B}{\partial x}. \quad (92)$$

The additional dimensions which correspond to the conjugate momenta p_x and p_y , are redundant, but allow a Hamiltonian description of the dynamics and the use of symplectic HDNNs. Then by imposing the constraints explicitly, we enforce the trajectories to respect the Hamiltonian dynamics so that phase-space volumes are preserved by the Hamiltonian flow. Essentially, this amounts to imposing the dynamical equations of the guiding-center motion twice in the loss function. The first time through the dynamical equation residual term and the second time through the regularization term which involves the vector potential. Note that the vector potential does not appear in the equations of motion (75)–(77) but it does appear in the Lagrangian variational integrators (e.g. [40]).

Again the loss function that is minimized during the training is given by (34) with $\mathbf{z}(t) = (x(t), y(t), p_x(t), p_y(t))$. The dynamical equations are (89)–(92) and the regularization term \mathcal{L}_{reg} contains the total Hamiltonian (88) and the constraints $\Phi_1 = p_x - A_x$ and $\Phi_2 = p_y - A_y$. For the numerical experiments of this section we used the same HDNN architecture as in the previous section, i.e. 4 hidden layers with 80 neurons per layer. The network was trained for 20000 epochs and for its training 1000 discrete time points were used in a normalized time domain $t \in [0, 200\pi]$. In Fig. 9, we present a time window of the x and y time series for the NN solution alongside the exact solution and the RK45 numerical solution. The training time for the NN is 13.2 minutes, whereas the RK45 method only requires 0.027 seconds. It is worth noting that, unlike the previous examples, here the HDNN provides a good approximation of the solution even in time intervals outside the training set, as illustrated in Figs. 9 and 11. The network not only accurately predicts the guiding center trajectory, but also conserves energy better than the RK45 method (Fig. 10).

Reapplying the dynamical equations for x and y , while considering the constraints Φ_1 and Φ_2 within \mathcal{L}_{reg} , results in a subtle enhancement in training efficiency, as illustrated in Fig. 12. Notably, the inclusion of the energy regularization term \mathcal{L}_{en} plays a crucial role in achieving remarkable conservation of energy when compared to the non-symplectic RK45 method. This finding provides evidence that symplectic neural network algorithms can serve as valuable tools for conservative and structure-preserving integration of particle and guiding center orbits in tokamak plasmas. In future work, we plan to extend this methodology to compute guiding center orbits in realistic fusion-relevant magnetic field topologies.

5 Conclusions

In this study, we applied the Dirac method of constraints to enforce holonomic constraints in Hamiltonian systems. The constrained dynamics were computed by solving Hamilton-Dirac equations using physics-informed neural networks, termed HDNNs (Hamilton-Dirac neural networks). In addition, we applied the Dirac algorithm also on a problem with singular Lagrangian, specifically examining the motion of a guiding center in a magnetic field.

The holonomically constrained systems examined in this study include the simple planar pendulum in Cartesian coordinates and a two-dimensional elliptically restricted harmonic oscillator. In both cases, HDNNs demonstrated superior accuracy compared to standard explicit algorithms like the RK45 method. They effectively conserved energy and preserved the Dirac constraints, unlike the standard explicit methods. These preservation properties were learned by the HDNNs through appropriate regularization terms in the total loss function, which was minimized during the training procedure. In the case of guiding center motion, enforcing energy conservation proved crucial for computing stable and accurate orbits, offering a significant advantage over standard explicit numerical solvers. Traditionally, ensuring

energy and phase space volume conservation relies on structure-preserving discretization of the Lagrangian density or the action function, leading to implicit numerical solvers with large computational times. Embedding the guiding center motion system in a higher-dimensional space (i.e., the phase space) affected only marginally the accuracy of learned solutions, but it offers the possibility to use the same HDNN architecture and to impose additional holonomic or phase-space constraints using the Dirac method.

While the computational time for training the networks exceeded that of explicit methods by many orders of magnitude, parallel computing capabilities and pretrained networks, such as generative pretrained models, can be leveraged to reduce this time. Future research will focus in utilizing advanced network architectures and types, such as echo state networks and generative pretrained models, for constrained systems. The study will also explore chaotic dynamics and further investigate the potential significance of equation-driven machine learning in systems with singular Lagrangians

Acknowledgements

The author would like to thank prof. George Throumoulopoulos for useful discussions. This work has received funding from the National Fusion Programme of the Hellenic Republic – General Secretariat for Research and Innovation.

References

- [1] B. J. Leimkuhler and R. D. Skeel, “Symplectic numerical integrators in constrained hamiltonian systems,” *Journal of Computational Physics*, vol. 112, no. 1, pp. 117–125, 1994, ISSN: 0021-9991. DOI: <https://doi.org/10.1006/jcph.1994.1085>. [Online]. Available: <https://www.sciencedirect.com/science/article/pii/S0021999184710850>.
- [2] L. Jay, “Symplectic partitioned runge–kutta methods for constrained hamiltonian systems,” *SIAM Journal on Numerical Analysis*, vol. 33, no. 1, pp. 368–387, 1996. DOI: [10.1137/0733019](https://doi.org/10.1137/0733019). [Online]. Available: <https://doi.org/10.1137/0733019>.
- [3] W. M. Seiler, “Numerical integration of constrained hamiltonian systems using dirac brackets,” *Mathematics of Computation*, vol. 68, no. 226, pp. 661–681, 1999, ISSN: 00255718, 10886842. [Online]. Available: <http://www.jstor.org/stable/2585050> (visited on 12/21/2023).
- [4] J. Fu, L. Zhang, S. Cao, C. Xiang, and W. Zao, “A symplectic algorithm for constrained hamiltonian systems,” *Axioms*, vol. 11, no. 5, 2022. DOI: [10.3390/axioms11050217](https://doi.org/10.3390/axioms11050217). [Online]. Available: <https://www.mdpi.com/2075-1680/11/5/217>.
- [5] P. L. Kinon, P. Betsch, and S. Schneider, “Structure-preserving integrators based on a new variational principle for constrained mechanical systems,” *Nonlinear Dynamics*, pp. 14 231–14 261, 2023. DOI: [10.1007/s11071-023-08522-7](https://doi.org/10.1007/s11071-023-08522-7). [Online]. Available: <https://doi.org/10.1007/s11071-023-08522-7>.
- [6] P. A. M. Dirac, “Generalized hamiltonian dynamics,” *Canadian Journal of Mathematics*, vol. 2, pp. 129–148, 1950. DOI: [10.4153/CJM-1950-012-1](https://doi.org/10.4153/CJM-1950-012-1).
- [7] P. A. M. Dirac, “Generalized hamiltonian dynamics,” *Proceedings of the Royal Society of London. Series A, Mathematical and Physical Sciences*, vol. 246, no. 1246, pp. 326–332, 1958, ISSN: 00804630. [Online]. Available: <http://www.jstor.org/stable/100496> (visited on 12/22/2023).
- [8] K. Sundermeyer, *Constrained dynamics, Lecture notes in Physics 169*. Springer-Verlag, New York, 1982.

- [9] G. Flierl and P. Morrison, “Hamiltonian–dirac simulated annealing: Application to the calculation of vortex states,” *Physica D: Nonlinear Phenomena*, vol. 240, no. 2, pp. 212–232, 2011, “Nonlinear Excursions” Symposium and Volume in Physica D to honor Louis N. Howard’s scientific career, ISSN: 0167-2789. DOI: <https://doi.org/10.1016/j.physd.2010.08.011>. [Online]. Available: <https://www.sciencedirect.com/science/article/pii/S0167278910002502>.
- [10] G. R. Flierl, P. J. Morrison, and R. Vilasur Swaminathan, “Jovian vortices and jets,” *Fluids*, vol. 4, no. 2, 2019. [Online]. Available: <https://www.mdpi.com/2311-5521/4/2/104>.
- [11] K. Hornik, M. Stinchcombe, and H. White, “Multilayer feedforward networks are universal approximators,” *Neural Networks*, vol. 2, no. 5, pp. 359–366, 1989, ISSN: 0893-6080. DOI: [https://doi.org/10.1016/0893-6080\(89\)90020-8](https://doi.org/10.1016/0893-6080(89)90020-8).
- [12] M. Raissi, P. Perdikaris, and G. Karniadakis, “Physics-informed neural networks: A deep learning framework for solving forward and inverse problems involving nonlinear partial differential equations,” *Journal of Computational Physics*, vol. 378, pp. 686–707, 2019, ISSN: 0021-9991. DOI: <https://doi.org/10.1016/j.jcp.2018.10.045>. [Online]. Available: <https://www.sciencedirect.com/science/article/pii/S0021999118307125>.
- [13] I. Lagaris, A. Likas, and D. Fotiadis, “Artificial neural networks for solving ordinary and partial differential equations,” *IEEE Transactions on Neural Networks*, vol. 9, no. 5, pp. 987–1000, 1998. DOI: [10.1109/72.712178](https://doi.org/10.1109/72.712178).
- [14] J. Sirignano and K. Spiliopoulos, “Dgm: A deep learning algorithm for solving partial differential equations,” *Journal of Computational Physics*, vol. 375, pp. 1339–1364, 2018, ISSN: 0021-9991. DOI: <https://doi.org/10.1016/j.jcp.2018.08.029>. [Online]. Available: <https://www.sciencedirect.com/science/article/pii/S0021999118305527>.
- [15] S. Cuomo, V. S. Di Cola, F. Giampaolo, G. Rozza, M. Raissi, and F. Piccialli, “Scientific machine learning through physics-informed neural networks: Where we are and what’s next,” *Journal of Scientific Computing*, vol. 92, p. 88, 2022. DOI: [10.1007/s10915-022-01939-z](https://doi.org/10.1007/s10915-022-01939-z). [Online]. Available: <https://doi.org/10.1007/s10915-022-01939-z>.
- [16] G. E. Karniadakis, I. G. Kevrekidis, L. Lu, P. Perdikaris, S. Wang, and L. Yang, “Physics-informed machine learning,” *Nature Reviews Physics*, vol. 3, pp. 422–440, 2021. DOI: [10.1038/s42254-021-00314-5](https://doi.org/10.1038/s42254-021-00314-5). [Online]. Available: <https://doi.org/10.1038/s42254-021-00314-5>.
- [17] X.-Y. Guo and S.-E. Fang, “Structural parameter identification using physics-informed neural networks,” *Measurement*, vol. 220, p. 113 334, 2023, ISSN: 0263-2241. DOI: <https://doi.org/10.1016/j.measurement.2023.113334>. [Online]. Available: <https://www.sciencedirect.com/science/article/pii/S0263224123008989>.
- [18] D. A. Kaltsas and G. N. Throumoulopoulos, “Neural network tokamak equilibria with incompressible flows,” *Physics of Plasmas*, vol. 29, no. 2, p. 022 506, 2022. DOI: [10.1063/5.0073033](https://doi.org/10.1063/5.0073033). [Online]. Available: <https://doi.org/10.1063/5.0073033>.
- [19] R. Francesco, P. Stefano, C. Alessandro, L. Alessandro, and Q. Alfio, “A physics-informed multi-fidelity approach for the estimation of differential equations parameters in low-data or large-noise regimes,” *Atti Accad. Naz. Lincei Cl. Sci. Fis. Mat. Natur.*, vol. 32, pp. 437–470, 2021. DOI: [10.4171/RLM/943](https://doi.org/10.4171/RLM/943). [Online]. Available: <https://doi.org/10.4171/rlm/943>.

- [20] S. H. Rudy, S. L. Brunton, J. L. Proctor, and J. N. Kutz, “Data-driven discovery of partial differential equations,” *Science Advances*, vol. 3, no. 4, e1602614, 2017. DOI: [10.1126/sciadv.1602614](https://doi.org/10.1126/sciadv.1602614). [Online]. Available: <https://www.science.org/doi/abs/10.1126/sciadv.1602614>.
- [21] M. Raissi, P. Perdikaris, and G. E. Karniadakis, “Inferring solutions of differential equations using noisy multi-fidelity data,” *Journal of Computational Physics*, vol. 335, pp. 736–746, 2017, ISSN: 0021-9991. DOI: <https://doi.org/10.1016/j.jcp.2017.01.060>. [Online]. Available: <https://www.sciencedirect.com/science/article/pii/S0021999117300761>.
- [22] H. Qin, “Machine learning and serving of discrete field theories,” *Scientific Reports*, vol. 10, p. 19329, 2020. DOI: [10.1038/s41598-020-76301-0](https://doi.org/10.1038/s41598-020-76301-0). [Online]. Available: <https://doi.org/10.1038/s41598-020-76301-0>.
- [23] M. Mattheakis, D. Sondak, A. S. Dogra, and P. Protopapas, “Hamiltonian neural networks for solving equations of motion,” *Phys. Rev. E*, vol. 105, p. 065305, 6 Jun. 2022. DOI: [10.1103/PhysRevE.105.065305](https://doi.org/10.1103/PhysRevE.105.065305). [Online]. Available: <https://link.aps.org/doi/10.1103/PhysRevE.105.065305>.
- [24] M. Gelbrecht, N. Boers, and J. Kurths, “Neural partial differential equations for chaotic systems,” *New Journal of Physics*, vol. 23, no. 4, p. 043005, Apr. 2021. DOI: [10.1088/1367-2630/abeb90](https://doi.org/10.1088/1367-2630/abeb90). [Online]. Available: <https://dx.doi.org/10.1088/1367-2630/abeb90>.
- [25] S. Greydanus, M. Dzamba, and J. Yosinski, “Hamiltonian neural networks,” *Advances in Neural Information Processing Systems*, vol. 32, pp. 15379–15389, 2019. [Online]. Available: <https://arxiv.org/abs/1906.01563>.
- [26] T. Bertalan, F. Dietrich, I. Mezić, and I. G. Kevrekidis, “On learning Hamiltonian systems from data,” *Chaos: An Interdisciplinary Journal of Nonlinear Science*, vol. 29, no. 12, p. 121107, 2019. DOI: [10.1063/1.5128231](https://doi.org/10.1063/1.5128231). [Online]. Available: <https://doi.org/10.1063/1.5128231>.
- [27] C. Miles, G. Sam, H. Stephan, B. Peter, S. David, and H. Shirley, “Lagrangian neural networks,” *ICLR 2020 Deep Differential Equations Workshop*, 2020. [Online]. Available: <https://doi.org/10.48550/arXiv.2003.04630>.
- [28] A. Choudhary, J. F. Lindner, E. G. Holliday, S. T. Miller, S. Sinha, and W. L. Ditto, “Physics-enhanced neural networks learn order and chaos,” *Phys. Rev. E*, vol. 101, p. 062207, 6 2020. DOI: [10.1103/PhysRevE.101.062207](https://doi.org/10.1103/PhysRevE.101.062207). [Online]. Available: <https://link.aps.org/doi/10.1103/PhysRevE.101.062207>.
- [29] S. A. Desai, M. Mattheakis, and S. J. Roberts, “Variational integrator graph networks for learning energy-conserving dynamical systems,” *Phys. Rev. E*, vol. 104, p. 035310, 3 Sep. 2021. DOI: [10.1103/PhysRevE.104.035310](https://doi.org/10.1103/PhysRevE.104.035310). [Online]. Available: <https://link.aps.org/doi/10.1103/PhysRevE.104.035310>.
- [30] M. Finzi, K. A. Wang, and A. G. Wilson, “Simplifying hamiltonian and lagrangian neural networks via explicit constraints,” *ArXiv*, vol. abs/2010.13581, 2020. [Online]. Available: <https://api.semanticscholar.org/CorpusID:225067856>.
- [31] A. White, N. Kilbertus, M. Gelbrecht, and N. Boers, “Stabilized neural differential equations for learning constrained dynamics,” *ArXiv*, vol. abs/2306.09739, 2023. [Online]. Available: <https://api.semanticscholar.org/CorpusID:259187905>.
- [32] H. Jiequn, J. Arnulf, and E. Weinan, “Solving high-dimensional partial differential equations using deep learning,” *Proceedings of the National Academy of Sciences of the United States of America*, vol. 115, pp. 8505–8510, 2018. DOI: <https://doi.org/10.1073/pnas.1718942115>.

- [33] Y. Chen and S. Koohy, “Gpt-pinn: Generative pre-trained physics-informed neural networks toward non-intrusive meta-learning of parametric pdes,” *Finite Elements in Analysis and Design*, vol. 228, p. 104047, 2024. DOI: <https://doi.org/10.1016/j.finel.2023.104047>. [Online]. Available: <https://www.sciencedirect.com/science/article/pii/S0168874X23001403>.
- [34] R. G. Littlejohn, “Variational principles of guiding centre motion,” *Journal of Plasma Physics*, vol. 29, no. 1, pp. 111–125, 1983. DOI: [10.1017/S002237780000060X](https://doi.org/10.1017/S002237780000060X).
- [35] H. K. Wimmel, *Zeitschrift für Naturforschung A*, vol. 38, no. 6, pp. 601–607, 1983. DOI: [doi:10.1515/zna-1983-0601](https://doi.org/10.1515/zna-1983-0601). [Online]. Available: <https://doi.org/10.1515/zna-1983-0601>.
- [36] D. Pfirsch, *Zeitschrift für Naturforschung A*, vol. 39, no. 1, pp. 1–8, 1984. DOI: [doi:10.1515/zna-1984-0102](https://doi.org/10.1515/zna-1984-0102). [Online]. Available: <https://doi.org/10.1515/zna-1984-0102>.
- [37] H. K. Wimmel, “Kinetic guiding-center equations for the theory of drift instabilities and anomalous transport,” *Physica Scripta*, vol. 29, no. 2, p. 141, Feb. 1984. DOI: [10.1088/0031-8949/29/2/009](https://doi.org/10.1088/0031-8949/29/2/009). [Online]. Available: <https://dx.doi.org/10.1088/0031-8949/29/2/009>.
- [38] W. M. Seiler and R. W. Tucker, “Involution and constrained dynamics. i. the dirac approach,” *Journal of Physics A: Mathematical and General*, vol. 28, no. 15, p. 4431, Aug. 1995. DOI: [10.1088/0305-4470/28/15/022](https://doi.org/10.1088/0305-4470/28/15/022). [Online]. Available: <https://dx.doi.org/10.1088/0305-4470/28/15/022>.
- [39] M. D. Ardema, *Analytical Dynamics Theory and Applications*. Springer New York, 2005. DOI: <https://doi.org/10.1007/b116020>.
- [40] H. Qin and X. Guan, “Variational symplectic integrator for long-time simulations of the guiding-center motion of charged particles in general magnetic fields,” *Phys. Rev. Lett.*, vol. 100, p. 035006, 3 Jan. 2008. DOI: [10.1103/PhysRevLett.100.035006](https://doi.org/10.1103/PhysRevLett.100.035006). [Online]. Available: <https://link.aps.org/doi/10.1103/PhysRevLett.100.035006>.
- [41] J. E. Marsden and M. West, “Discrete mechanics and variational integrators,” *Acta Numerica*, vol. 10, pp. 357–514, 2001. DOI: [10.1017/S096249290100006X](https://doi.org/10.1017/S096249290100006X).
- [42] C. L. Ellison, J. M. Finn, J. W. Burby, M. Kraus, H. Qin, and W. M. Tang, “Degenerate variational integrators for magnetic field line flow and guiding center trajectories,” *Physics of Plasmas*, vol. 25, no. 5, p. 052502, 2018. DOI: [10.1063/1.5022277](https://doi.org/10.1063/1.5022277). [Online]. Available: <https://doi.org/10.1063/1.5022277>.
- [43] P. J. Morrison, “Structure and structure-preserving algorithms for plasma physics,” *Physics of Plasmas*, vol. 24, no. 5, p. 055502, 2017. DOI: [10.1063/1.4982054](https://doi.org/10.1063/1.4982054). [Online]. Available: <https://doi.org/10.1063/1.4982054>.
- [44] D. Pfirsch and P. J. Morrison, “The energy-momentum tensor for the linearized Maxwell–Vlasov and kinetic guiding center theories,” *Physics of Fluids B: Plasma Physics*, vol. 3, no. 2, pp. 271–283, 1991. DOI: [10.1063/1.859735](https://doi.org/10.1063/1.859735). [Online]. Available: <https://doi.org/10.1063/1.859735>.

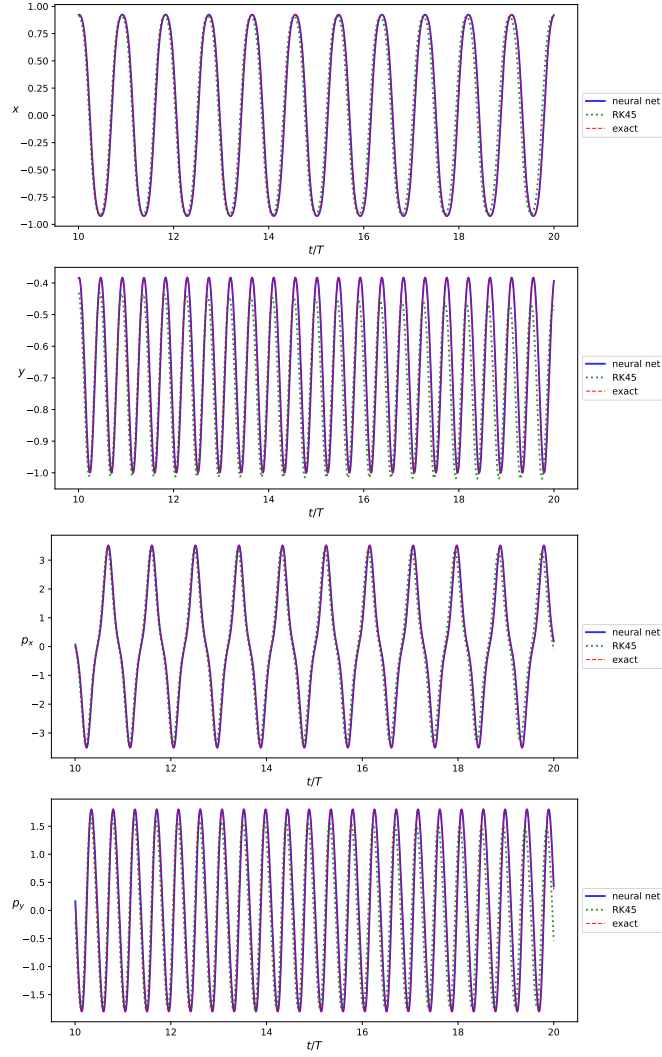


Figure 1: time series produced by the HDNN solution (33) for the canonical variables (x, y, p_x, p_y) (blue solid line) compared with the “exact solution” which is produced by the LSODA algorithm using a dense time grid (dashed red line) and the classical RK45 method (green dotted line). The solutions are displayed in the time window $t \in [10T, 20T]$. It is evident that the RK45 solution dissipates the energy as height and the momentum of the pendulum gradually decrease. On the other hand the HDNN solution reproduce the exact motion with high fidelity.

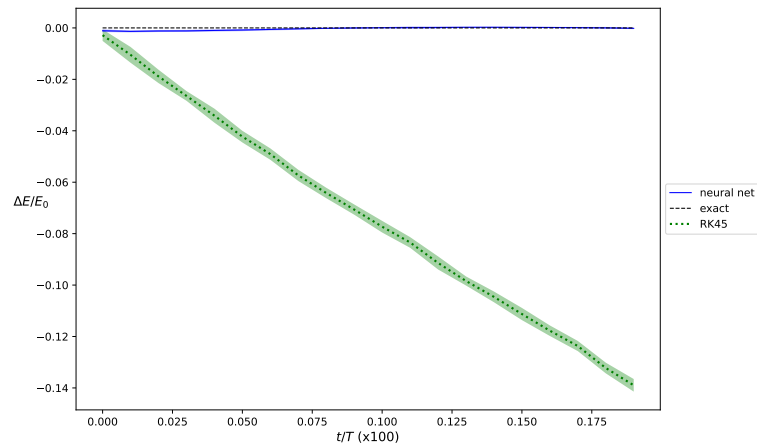


Figure 2: Energy drift diagram displaying the evolution of the quantity $(E(t) - E_0)/E_0$ for the simple pendulum. We have plotted the mean value of $\Delta E/E_0$ along its standard deviation in batches of 100 time steps. Blue line corresponds to the HDNN solution while the green line is the RK45 solution. Evidently, the HDNN conserves the energy, while RK45 produces spurious dissipation.

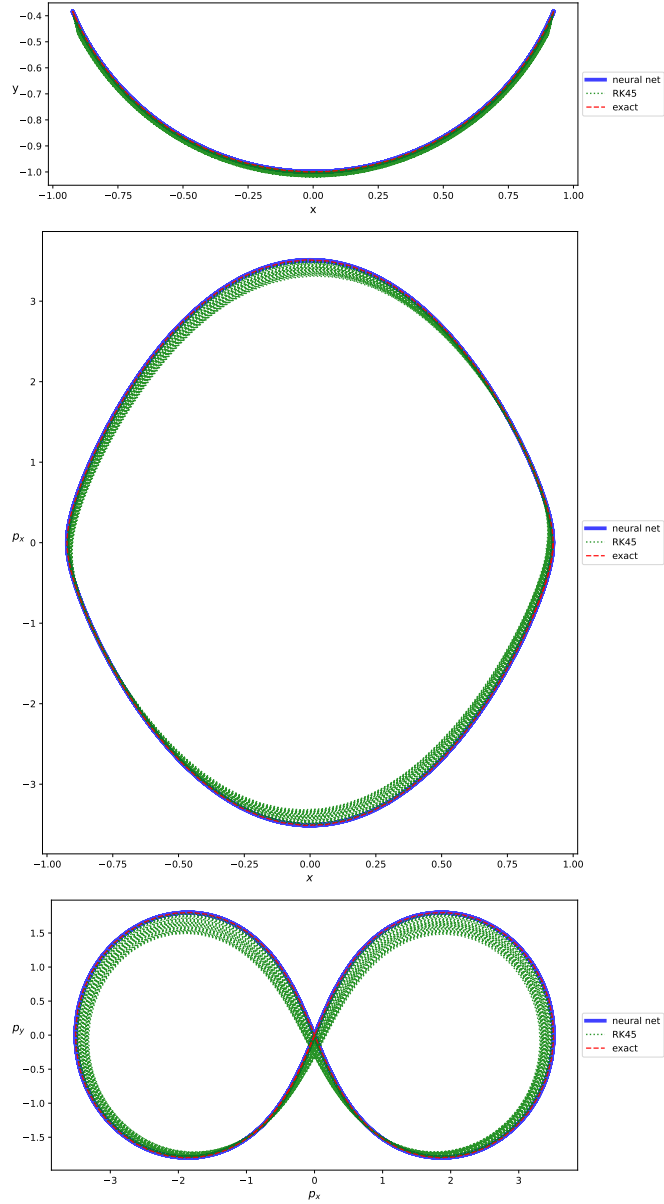


Figure 3: The trajectories of the HDNN (blue solid line) and the RK45 (green dots) solutions on the sections (x, y) (top), (x, p_x) (middle) and (p_x, p_y) (bottom), compared with the exact trajectories (red dashed line). It is clear that the HDNN solution stays on the exact trajectories during the entire time evolution while the RK45 solution drifts away.

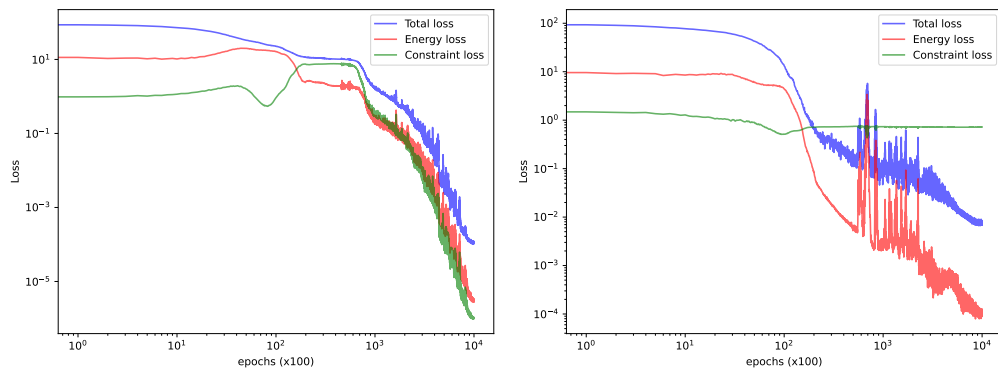


Figure 4: The loss history for the constrained optimization (left) versus the unconstrained minimization (right). The total loss (blue line) is displayed along with the energy (red line) and the constraint (green line) terms of the loss function. Clearly, imposing the Dirac constraints facilitates the minimization of the loss function so the network can learn the dynamics more efficiently.

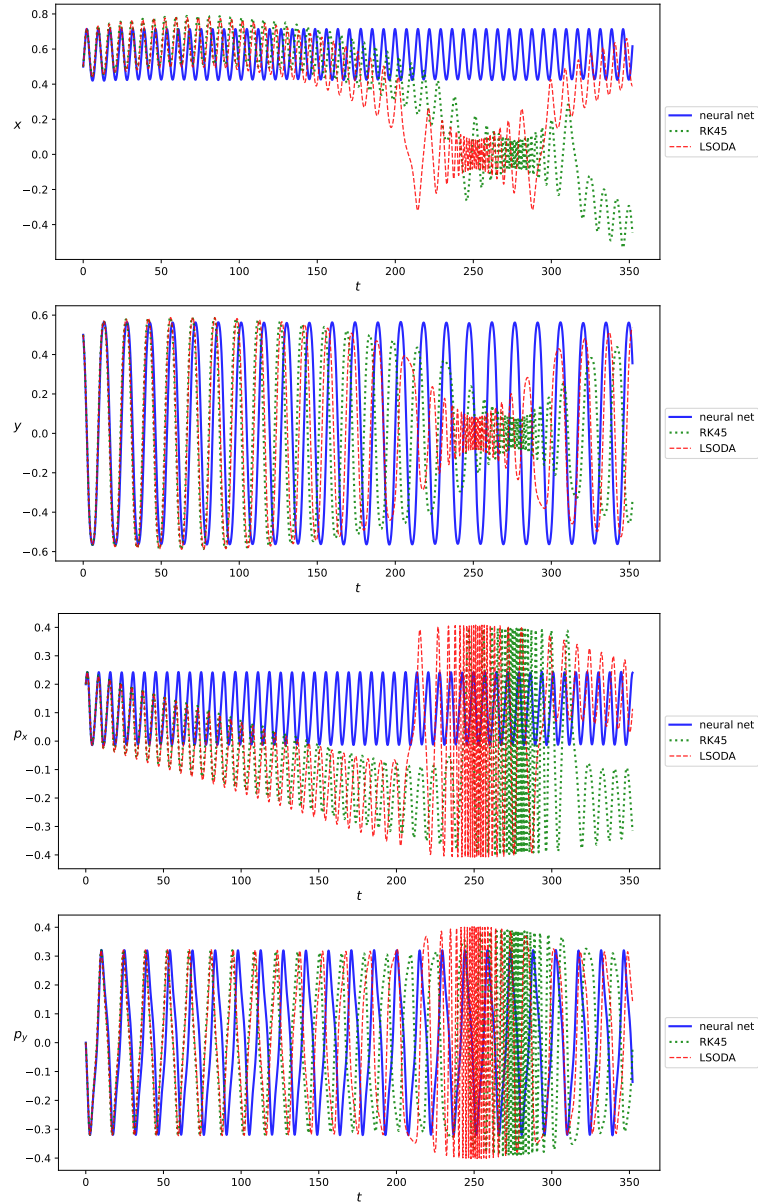


Figure 5: time series for the elliptically restricted harmonic oscillator computed by the HDNN, LSODA and RK45 methods. The standard numerical approaches exhibit unphysical behavior, while the HDNN solution remains stable over the entire time domain.

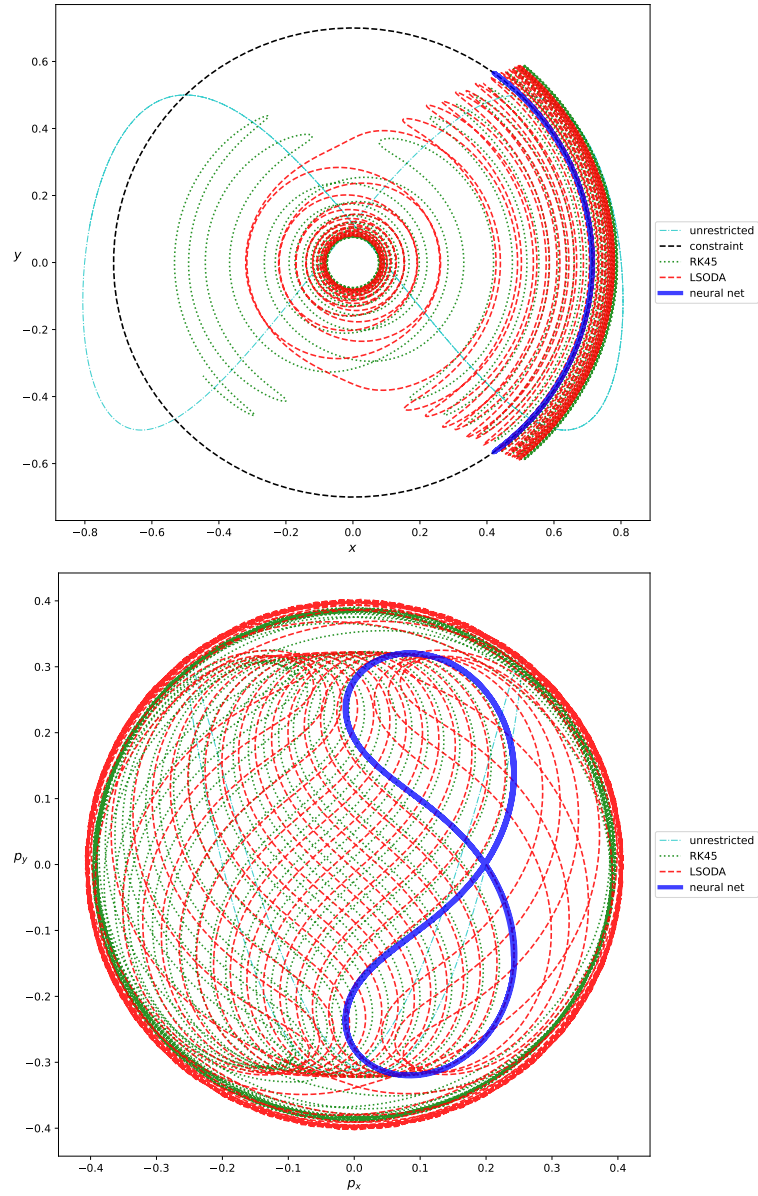


Figure 6: The trajectories of the elliptically restricted harmonic oscillator as computed by the NN solution and the RK45 and LSODA methods on the $x - y$ and $p_x - p_y$ planes, along with the corresponding unrestricted trajectories. Evidently, the NN solution adheres to constraints, while standard numerical solutions do not.

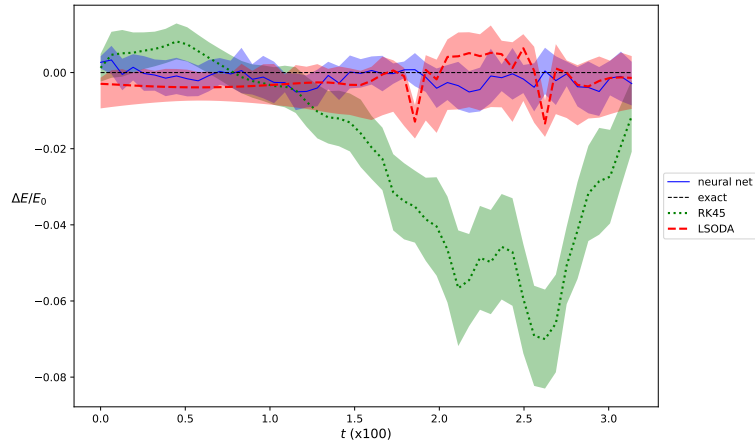


Figure 7: time series of the quantity $\Delta E/E_0$, representing the energy drift, for three numerical solutions. Both the HDNN and the LSODA algorithm maintain the system's energy, while the RK45 solution exhibits significant drift. The diagram displays mean values computed in batches of 50 grid points, along with their standard deviation.

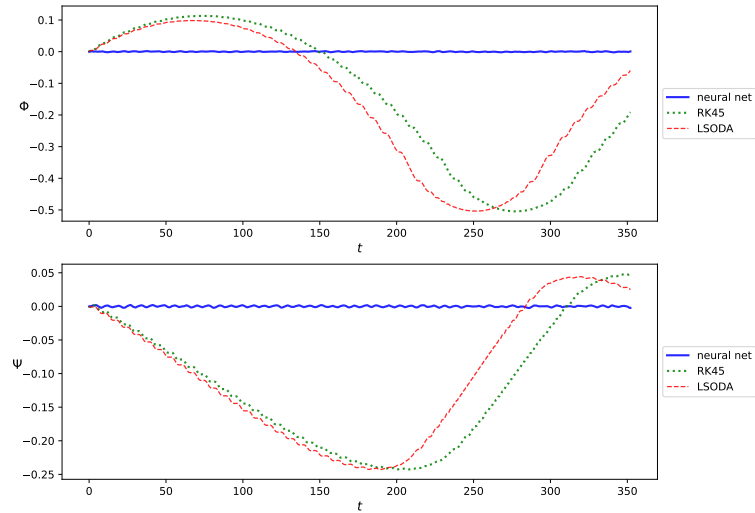


Figure 8: Evolution of constraint functions Φ and Ψ for HDNN, LSODA, and RK45 solutions. HDNN exhibits superior accuracy in satisfying Dirac constraints compared to the other numerical methods.

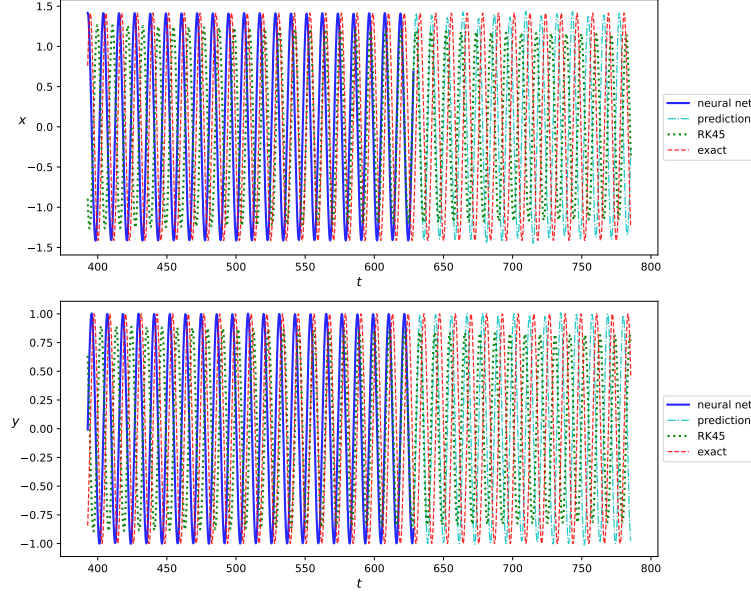


Figure 9: time series for the x and y coordinates of the guiding center motion in the magnetic field (74) in the time window $t \in [390, 785]$. The trained NN solution (blue solid line) is collated with the RK45 (green dotted line) and the exact solution (red dashed line). The training interval is $t \in [0, 628]$, therefore part of the time series displays the prediction (extrapolation) of the NN in the interval $[628, 785]$ (cyan dot-dashed line). Clearly the NN solution preserves the amplitude of the guiding center elliptical motion.

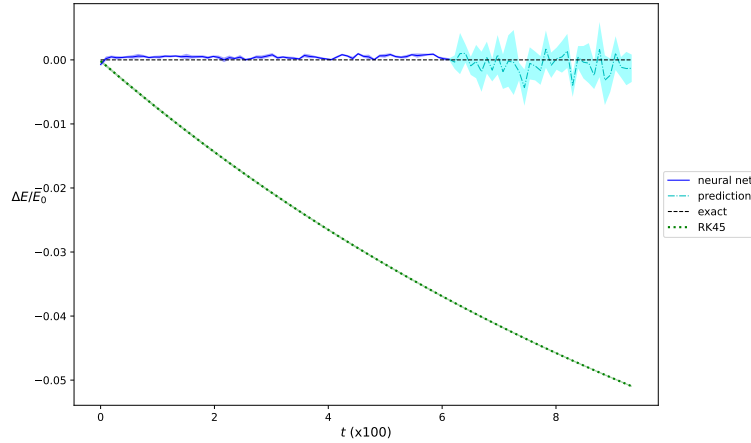


Figure 10: Evolution of the mean value and standard deviation of the quantity $\Delta E/E_0$ computed in batches of 100 time steps. This quantifies the energy drift for the trained NN solution (blue solid line) and the NN prediction (cyan dot-dashed line) and the RK45 solution (green dotted line) in the time interval $[0, 940]$. The trained NN and remarkably the NN prediction (extrapolation) conserve the energy of the GC motion in contrast with the RK45 solution which suffers from unphysical dissipation.

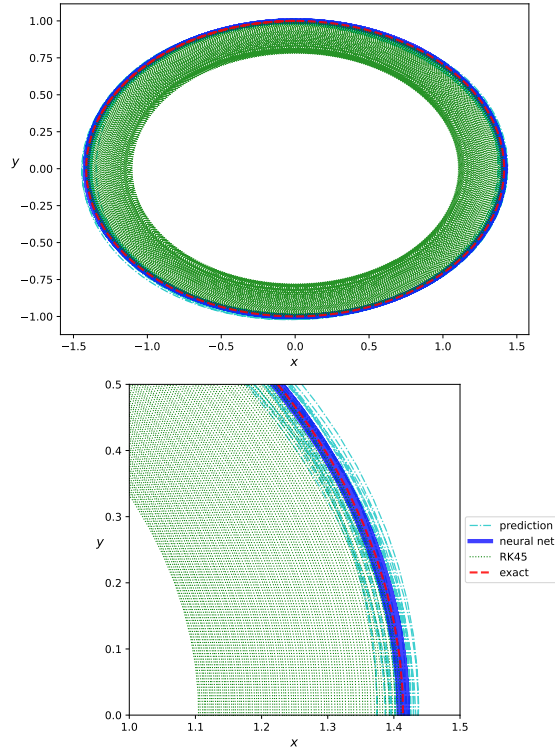


Figure 11: The trajectory of the guiding center in the magnetic field (74) as constructed by the trained NN solution (solid blue line), and the RK45 solution (green dotted line) collated with the exact trajectory (red dashed line). The cyan dot-dashed line represents the predicted part of the trajectory after the training interval. The trained NN solution lies exactly upon the exact trajectory while the RK45 solution drifts towards the centre of the elliptical orbit due to the spurious dissipation of the energy.

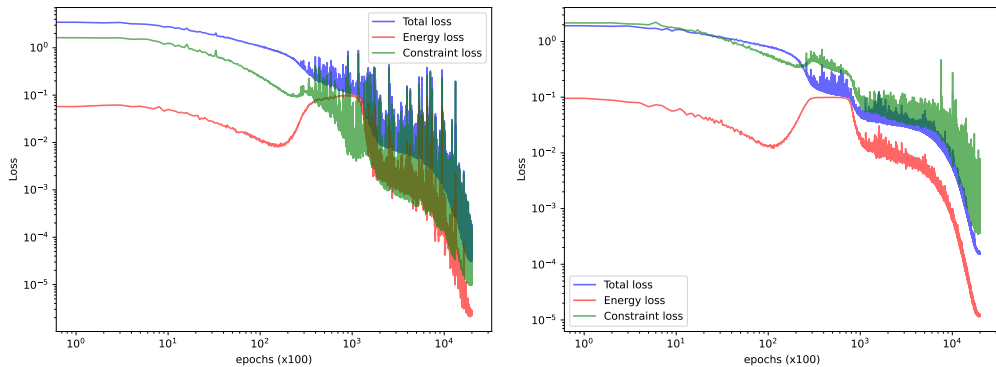


Figure 12: Training history of the loss function versus the number of training epochs for the constrained minimization (left) and the unconstrained minimization (right). The imposition of the Dirac constraints slightly facilitates the minimization of the loss and thus enhances the training efficiency.